Journal of Alloys and Compounds 594 (2014) 189–196

Contents lists available at ScienceDirect

Journal of Alloys and Compounds

journal homepage: www.elsevier.com/locate/jalcom

Ionic exchange and the local structure in the HfO_2/Ho_2O_3 system studied by PAC spectroscopy

D. Richard [a,*], G.N. Darriba [a], E.L. Muñoz [a], L.A. Errico [a,b], M. Rentería [a]

[a] Departamento de Física and Instituto de Física La Plata (IFLP, CONICET La Plata), Facultad de Ciencias Exactas, Universidad Nacional de La Plata, C.C. 67, 1900 La Plata, Argentina
[b] Universidad Nacional del Noroeste de la Provincia de Buenos Aires (UNNOBA), Monteagudo 2772, 2700 Pergamino, Buenos Aires, Argentina

ARTICLE INFO

Article history:
Received 19 December 2013
Accepted 16 January 2014
Available online 24 January 2014

Keywords:
Rare earth alloys and compounds
Mechanical alloying
Solid state reactions
Hyperfine interactions
Impurities in semiconductors
Perturbed angular correlations, PAC

ABSTRACT

The ionic exchange of Hf and Ho atoms in the HfO_2/Ho_2O_3 system was studied at the atomic level applying the nuclear solid-state Time-Differential γ–γ Perturbed-Angular-Correlation (PAC) spectroscopy. This exchange was promoted by a ball-milling-assisted solid-state reaction between Ho_2O_3 and *m*-HfO_2 initial powders. In order to follow and to elucidate the effect of different variables (milling time, temperature, pressure) on the exchange process and the appearance of new phases, $^{181}Hf(\rightarrow{}^{181}Ta)$ ions were used as local probes in the PAC experiments. The measured hyperfine interactions enabled the electric-field gradient tensor (EFG) characterization at Hf sites at each step of the process. At the final stages of the solid-state reaction, 75–90% Hf-doping at both substitutional defect-free cation sites of Ho_2O_3 was achieved, being the EFG measured at these sites in excellent agreement with those determined in ^{181}Hf-implanted Ho_2O_3 samples and to those predicted by the EFG systematics established in rare-earth *bixbyites* doped by ion-implantation of $^{181}Hf(\rightarrow{}^{181}Ta)$ ions. *Ab initio* electronic structure calculations of the EFG at Ta impurities localized at both cation sites in Ho_2O_3 also confirm the ^{181}Hf cationic substitution in both PAC experiments. Additional *ab initio* calculations at Hf impurity sites in Ho_2O_3 and Tm_2O_3 were performed to study the relative Hf preference for the symmetric site of the structure. We showed that high-energy milling plus high temperature treatments are both necessary to achieve a high degree of Hf substitution in the cation sublattice of the Ho_2O_3 structure. Also, we found that the pressure effect on the crystal structure favors the impurity substitution at cationic sites closer to a homogenous distribution of the probes and with much less local and far disorder. Additional spurious hyperfine interactions that were always present in ^{181}Hf-implanted Ho_2O_3 samples were not observed when using this solid-state reaction method. The appearance of a modified *m*-HfO_2 phase produced after heavy Ho-doping was also discussed.

1. Introduction

Impurities play a fundamental role in semiconductor physics. When semiconducting oxides are doped with appropriate impurities the resulting compound can develop new and unexpected physical properties, which could have important technological applications (see, e.g., Refs. [1–3], and references therein). Thus, the understanding and the accurate determination of electronic and structural properties of doped semiconductor oxides is of paramount importance. One successful approach to do this is to measure physical quantities on doped semiconductors that nowadays can also be accurately calculated using *ab initio* density-functional-theory electronic structure calculations [4–9].

The rare-earth (RE) oxide Ho_2O_3 is a wide band-gap semiconductor with an energy gap of 5.3 eV [10]. Hence, it should be colorless; nevertheless, it is a pale yellow powder due to many lattice defects such as oxygen vacancies, which are commonly present in powder samples. This sesquioxide crystallizes in the structure of the mineral *bixbyite* and has many technological applications in catalysis [11,12], in the calibration of spectrophotometers, as a dopant in ceramics [13] and glass [14], in thin film-based capacitors [15], etc. In the last few years HfO_2 and different RE oxides have been deeply studied because of their potential use in Si-based semiconductor technology as a substitute of SiO_2 in metal-oxide-semiconductor field-effect transistors (MOSFETs) [16,17]. To improve the key properties of HfO_2 and RE oxides in MOSFET technology, different configurations such as Gd-doped HfO_2 and HfO_2/Gd_2O_3/Si stacks have been investigated very recently [18,19]. Among the series of RE oxides, Ho_2O_3 have attracted much attention as a promising candidate for ion-sensitive field-effect transistor (ISFET) devices [20] and other MOSFETs, because it is a high-*k* dielectric, with a wide energy band gap, high resistivity, chemical and thermal stability with Si, and possible

* Corresponding author. Tel.: +54 221 4246062; fax: +54 221 4252006.
E-mail address: richard@fisica.unlp.edu.ar (D. Richard).

http://dx.doi.org/10.1016/j.jallcom.2014.01.107
0925-8388/

reduced leakage current [21]. In this sense, it is relevant to study the local structure of the possible phases that could be developed at HfO_2/Ho_2O_3 interphases, as well as the ionic exchange between Hf and Ho ions in their respective oxide matrices, when both oxides are grown in close contact.

Different experimental techniques, such as Nuclear Quadrupole Resonance (NQR), Nuclear Magnetic Resonance (NMR), Mössbauer Spectroscopy (MS), and Time-Differential γ–γ Perturbed-Angular-Correlation (PAC) spectroscopy, can be employed to study local electronic and structural properties at suitable probe-atom sites [22–24]. In particular, PAC has been extensively applied to study doped materials from the point of view of solid-state physics, chemistry, and biology in order to elucidate the subnanoscopic environment(s) of constituent or impurity atoms in solids, and the nature of chemical bonding in different kind of molecules and compounds [4,5,25–34].

PAC is a nuclear solid-state spectroscopy that enables a high resolution determination of a physical local quantity, the electric-field-gradient (EFG) tensor, at the site of a probe-atom adequately introduced (by means of ion implantation, thermal diffusion, or chemical preparation, among other methods) in the system under study. The power of PAC lies in its highly local sensitivity (due to the r^{-3} dependence of the EFG from their charge sources), which gives access to structures on the atomic scale. Additionally, the physical principles of PAC allow to carry out the experiments under a wide range of suitable external conditions (different temperatures, pressures, atmospheres, etc.), enabling to extract information concerning crystal structures, nanoscopic characterization of disperse species or coexistent compound phases, charge-density symmetry, charge-exchange mechanisms, solid-state phase transitions, absolute populations of nonequivalent lattice sites, etc., at the precise site of the impurity. For these reasons, PAC could be used as a powerful tool in order to study the local and non-local changes induced by thermally activated inter-diffusion mechanisms between oxides assisted, e.g., by mechanical alloying. Being the radioactive ^{181}Hf isotope the second most used PAC probe, it seems natural to investigate the applicability of this experimental technique to the study of the HfO_2–Ho_2O_3 inter-diffusion mechanisms.

One method to produce doped materials, which is also an easy way to reproduce phases and compounds that could be developed at the interphases in MOSFETs fabricated by standard methods, is mechanical alloying in combination with thermal treatments. This simple preparation method can synthesize a variety of equilibrium and non-equilibrium alloy phases and compounds. In this method, high-energy mills are used and the starting materials are repeatedly submitted to deformation, welding, fracturing, and rewelding. During this process, the powder particles are grinded and the microstructure is refined up to the nanoscopic scale, giving rise to inter-diffusion and mixing of the reacting elements. The way mixing occurs was the subject of different studies and models (see, e.g., Ref. [35] and references therein). Ball-milling could be a low-cost alternative to other doping methods as, e.g., the implantation of impurities by ion acceleration, enabling easily high doses of the dopants when these are needed. Additionally, the thermal treatments can also introduce structural and chemical local changes at the atomic sites. In order to clarify the role played by each step of the desired solid-state reaction, it is necessary to obtain experimental information on the way mixing and inter-diffusion proceed.

In this work we focused on different aspects of the doping process of Hf donor impurities in the wide-gap Ho_2O_3 semiconductor, using a ball-milling-assisted solid-state reaction between neutron-activated m-HfO_2 (hence, having some radioactive ^{181}Hf tracers together with the inactive Hf atoms) and the host oxide C-Ho_2O_3. In addition, the Ho doping in HfO_2 was also discussed, as a potential phase that can arise at HfO_2/Ho_2O_3 interphases. The efficiency of the ionic exchange between the Hf (Ho) impurities and the cations of the Ho_2O_3 (HfO_2) host was studied applying the local-scale PAC spectroscopy. The hyperfine interaction between the daughter nuclide of the ^{181}Hf probe-atom, the ^{181}Ta ion, and the extranuclear fields enables to monitor through a nonstandard approach the Hf impurity doping at the "eye-of-the-storm" of the ionic exchange process and, at the same time, how Ho atoms modifies the HfO_2 structure. Although this approach was already attempted in the literature to follow this kind of Hf doping process, up to now there not exist successful results besides the case of Hf-doped Tm_2O_3 [36]. Recent works have also used this approach starting from powder blends of HfO_2 and other oxides (such as SiO_2 [37] and La_2O_3 [38]), but the Hf doping into the oxide host was not achieved in these cases. In our experiments, PAC spectroscopy was used after each step of the doping process to characterize the different samples and to elucidate the effect of each variable (milling time, temperature, and pressure) on the ionic exchange. We showed the capability of the PAC spectroscopy to follow a doping process and to give information about the mixing and inter-diffusion processes. We also determined the absolute efficiency of the ball-milling-assisted solid-state reaction to locate Hf donor impurities at defect-free cationic sites of the Ho_2O_3 semiconductor.

Besides its relevance in condensed-matter basic research and in doping technology, the local characterization of Hf donor impurities in Ho_2O_3 obtained after a solid-state reaction between HfO_2 and Ho_2O_3 (as well as the inverse case, i.e., acceptor Ho impurities doping HfO_2) is necessary to undertake a broader study of potential phases that can arise at the interphase of the HfO_2/Ho_2O_3 stack system. This kind of simultaneous PAC study can only be done by this doping method.

2. Experimental

2.1. PAC spectroscopy

PAC spectroscopy is based on the conservation of angular momentum. Basically, this technique consists in the determination of the perturbation caused by extranuclear fields on the correlation between the emission directions of two successive radiations emitted during a nuclear-decay cascade. For a complete description of this technique see Refs. [22–24]. In order to perform the PAC experiments presented in this work we made use of the well known 133–482 keV γ–γ cascade in ^{181}Ta, produced after the β^- nuclear decay of the ^{181}Hf isotope. These experiments were performed using the PACAr spectrometer (a detailed description of this spectrometer can be found in Ref. [39]). To analyze the measured PAC spectra, $R(t)$, we used a multiple-site model of the perturbation factor $G_{22}(t)$, folded with the time resolution curve of the spectrometer. For pure nuclear-electric-quadrupole interactions, polycrystalline samples, and spin $I = 5/2$ of the intermediate nuclear level of the γ–γ cascade [22]:

$$R(t) \approx A_{22}^{\exp} G_{22}(t) = A_{22}^{\exp} \sum_i f_i (S_{20,i} + \sum_{n=1}^{3} [S_{2n,i} \cos(\omega_{n,i} t) e^{-\delta_i \omega_{n,i} t}]), \quad (1)$$

where $A_{22}^{\exp}$ is the experimental anisotropy of the γ–γ cascade, f_i is the relative fraction of nuclei that experiences a given perturbation, giving rise to the corresponding hyperfine interaction. The ω_n interaction frequencies are related to the experimentally determined nuclear-quadrupole frequency $\omega_Q = eQV_{zz}/40\hbar$ by $\omega_n = g_n(\eta)\omega_Q$. The g_n and S_{2n} coefficients are known functions of the asymmetry parameter $\eta = (V_{xx} - V_{yy})/V_{zz}$ [40], with V_{ii} the principal components of the traceless EFG tensor that are defined by the convention $|V_{xx}| \leq |V_{yy}| \leq |V_{zz}|$. According to this convention $0 \leq \eta \leq 1$. The exponential functions account for a lorentzian frequency distribution of relative width δ around ω_n, correlated with an EFG distribution due to slightly different surroundings of the ^{181}Ta probes. For PAC probes with $I = 5/2$, the ω_n frequencies corresponding for each hyperfine interaction appear as a triplet in the Fourier transform of the $R(t)$ spectrum, depending the positions of each of these peaks on the η and V_{zz} values.

2.2. Ho_2O_3 crystal structure

Holmium sesquioxide crystallizes in the cubic *bixbyite* phase, C-Ho_2O_3 ($a = 10.606(2)$ Å [41]), which is thermodynamically stable under around 2250 K [42]. In this structure the cations form a nearly cubic face-centered lattice (space group $Ia\bar{3}$), in which six out of the eight tetrahedral sites are occupied by oxygen

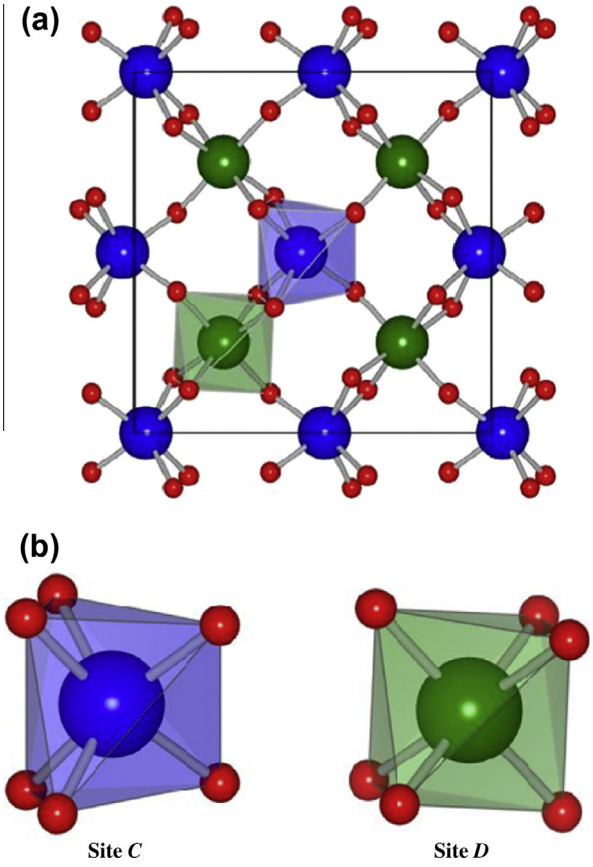

Fig. 1. (a) Unit cell layer of *C*-Ho_2O_3 along the [001] plane. Note the two nonequivalent cationic sites *C* and *D* (blue and green polyhedra, respectively). (b) Nearest-neighbor oxygen (small red spheres) distribution around each cationic site *C* and *D* (large blue and green spheres, respectively) in the *bixbyite* structure. (For interpretation of the references to color in this figure legend, the reader is referred to the web version of this article.)

atoms. The unit cell consists of eight such cubes, containing 32 holmium atoms and 48 oxygen atoms. Two nonequivalent sites for the cations, called *C* and *D*, both O_6-coordinated, characterize the structure (see Fig. 1a). Their relative abundance in the lattice is $f_C/f_D = 3$. Site *D* is axially symmetric and can be locally described as a Ho atom surrounded by six oxygen atoms localized at the corners of a distorted cube, leaving two corners of one body diagonal free (D_{3d} point-group symmetry) (see Fig. 1b). At this site, the six nearest neighbor oxygen atoms (O_{NN}) are at 2.283(3) Å from Ho [41]. In the case of site *C*, the cube is more distorted (C_2-symmetry) and the six oxygen atoms leave free two corners on a face diagonal of this cube (see Fig. 1b). At this site, the Ho–O_{NN} bond-lengths are grouped in three pairs of distances: 2.244(3) Å, 2.270(3) Å, and 2.337(3) Å [41]. According to the geometry of the structure we expect two clearly distinguishable hyperfine interactions: that corresponding to $^{181}Hf(\rightarrow{}^{181}Ta)$ probes located at site *C* will be characterized by a high η value (larger than 0.5), while $\eta_D \approx 0$ will characterize the axially symmetric site *D*. According to the relative abundance of each site in the lattice, the first interaction should be present with an intensity three times higher than the second one, if a homogenous distribution of the impurities occurs in the real samples.

2.3. m-HfO_2 crystal structure

Hafnium dioxide displays three crystalline phases at low pressure: monoclinic, tetragonal, and cubic. The monoclinic form, *m*-HfO_2, is stable up to around 1900 K [43]. The monoclinic unit cell (space group $P2_1/c$) has dimensions $a = 5.1170(1)$ Å, $b = 5.1754(2)$ Å, $c = 5.2915(2)$ Å, and $\beta = 99.216(2)^\circ$ [44] and contains four HfO_2 formula units. In this crystal structure, the four Hf atoms occupy equivalent positions and are sevenfold-coordinated with their O_{NN}, with Hf–O bond-lengths ranging between 2.03 and 2.25 Å (see Fig. 2). In PAC experiments in which ^{181}Ta probes are located at defect-free cation sites of pure *m*-HfO_2, it has been observed a dominant well-defined hyperfine interaction characterized by values close to $\omega_Q = 124$ Mrad/s and $\eta = 0.35$ [45,46].

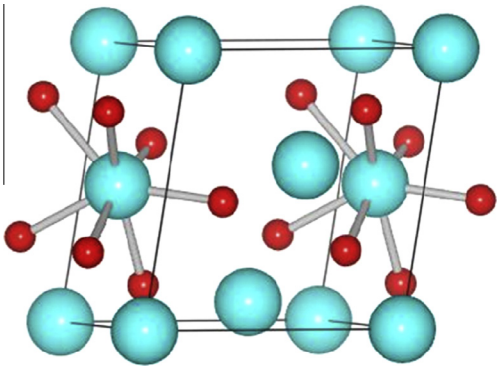

Fig. 2. Crystal structure of the *m*-HfO_2 phase. Small (red) and large (cyan) spheres represent oxygen and hafnium atoms, respectively. (For interpretation of the references to color in this figure legend, the reader is referred to the web version of this article.)

2.4. Sample preparation and PAC measurements

The starting materials for these experiments were 2 mg of *m*-HfO_2 (Aldrich, 98% of metallic purity) and 594.5 mg of *C*-Ho_2O_3 (Aldrich, 99.95% metallic purity). These amounts of initial powders were chosen to obtain a concentration of Hf impurities relative to Ho atoms up to 1.2 at.%. The *m*-HfO_2 powder was first encapsulated in air at atmospheric pressure in a sealed quartz tube and irradiated with thermal neutrons (with a flux of 2×10^{13} neutrons/cm^2 s) in the RA-3 reactor of the National Atomic Energy Commission (CNEA, Argentina) in order to obtain 300 μCi of ^{181}Hf activity by means of the nuclear reaction $^{180}Hf(n, \gamma)^{181}Hf$. The irradiated *m*-$HfO_2$ powder was annealed in air at 1123 K for 1 h to remove any possible radiation damage. As a first step of our study, the irradiated *m*-HfO_2 powder was characterized at room temperature (RT = 300 K) in air by γ–γ PAC.

Afterwards, the activated *m*-HfO_2 powder was manually mixed with the Ho_2O_3 powder and treated in air for 26 h at 1273 K and 6 h at 1523 K (labeled as "Sample I"). At the end of this thermal treatment the sample was charged into a cylindrical agate vial (10 cm^3 vol.) with 1 agate ball (1.2 cm diameter) under air atmosphere; the ball-to-powder weight ratio was 4. The ball-milling was performed in a horizontal oscillatory mill (Retsch MM2) with an operating cycle of 3 h. The milling frequency was 40(2) Hz ("Sample II"). As a next step of the process, one half of Sample II was thermally treated in air at atmospheric pressure for 26 h at 1273 K and 6 h at 1523 K ("Sample III"). The rest of Sample II was pressed as circular pellets under a pressure of 20 kN/m^2. Then, the pellet underwent the same thermal treatment as Sample III ("Sample IV"). PAC measurements were carried out in air at RT on Samples I–IV, immediately after their preparation. In addition, Samples III and IV were measured in air at 573 K.

3. Results and discussion

Let us first discuss the EFG characterization at ^{181}Ta impurities obtained at RT in air in PAC experiments implanting ^{181}Hf ions into Ho_2O_3 polycrystalline samples [47]. To obtain a complete characterization of all the hyperfine interactions observed in these experiments in order to use them as reference values for the ball-milling study, we reanalyzed the as-implanted and the after-annealing measurements. A study of the EFG temperature dependence and the discussion of other topics in the implanted samples (the comparison with the EFG results obtained with another probe, the applicability of different models for the EFG, etc.) can be found in Ref. [47].

The $R(t)$ spectra, and their corresponding Fourier transforms, are shown in Fig. 3. Solid lines in the $R(t)$ spectra are the best least-squares fits of Eq. (1) to the experimental data. Solid lines in the Fourier spectra are the Fourier transformations of the corresponding $R(t)$ fits. The fitted parameters are listed in Table 1. As can be seen in Fig. 3, the as-implanted $R(t)$ spectrum is rather dampened, as usually occurs at this stage in ^{181}Hf-implanted binary oxides [48–51], showing that the radiation damage produces a not negligible host disorder around the probe-atoms. Nevertheless, at the same time, the values of the hyperfine parameters and the almost homogenous distribution of the probes

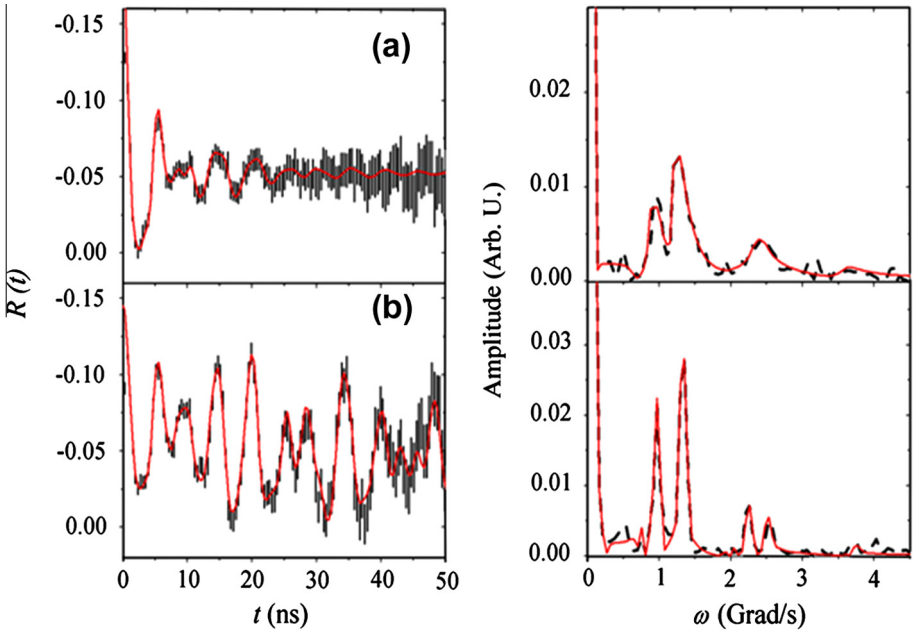

Fig. 3. $R(t)$ spectra (left) and their corresponding Fourier transformed spectra (right) of ^{181}Hf($\rightarrow^{181}$Ta)-implanted C-Ho_2O_3 measured at RT in air (a) in the as-implanted stage and (b) after a thermal annealing in air at 1323 K for 2 h.

in the lattice (see Table 1, first two rows) show a high degree of impurity substitution at cationic sites. In effect, in the as-implanted Fourier spectrum it is possible to detect almost the same ω_n frequencies corresponding to the dominant interactions that will be found after the annealing treatments, but with a rather broad frequency distribution (see Fig. 3).

After the annealing treatment in air at 1323 K for 2 h, these two interactions are very well defined (their frequency distribution δ is drastically diminished) and the asymmetry parameter of HfiD is reduced to zero (axial symmetry), as expected for the coordination symmetry of site D. In the case of HfiC, a high η value was found, also in agreement with the coordination symmetry of site C. Furthermore, the frequency associated with the axially symmetric interaction is twice as large as the asymmetric one, as found previously for ^{181}Ta probes localized at both cationic sites in other sesquioxides with the *bixbyite* structure [51]. The relative intensity of the two hyperfine interactions should be $f_C/f_D = 3$ if the cationic sites were homogenously occupied according to their natural abundance in the crystalline structure. In the present experiment, the obtained ratio is smaller than this value ($f_C/f_D = 2.3$). This

Table 1
Fitted parameters of the hyperfine interactions observed in ^{181}Hf-implanted Ho_2O_3 experiments carried out at RT in air in the as-implanted and after-annealing samples.

		f (%)	ω_Q (Mrad/s)	η	δ (%)
As implanted	HfiC	62(6)	117(3)	0.54(3)	13(1)
	HfiD	38(3)	195(2)	0.21(2)	5.0(9)
After annealing	HfiC	53(4)	114.3(3)	0.611(4)	0.0(2)
	HfiD	23(5)	207.0(7)	0.00[a]	0.3(4)
	HfiX	12(3)	8(1)	1.00[a]	0(1)
	HfiY	12(2)	111(1)	0.22(3)	0.0(9)

[a] When no errors are quoted the parameter was kept fixed.

Table 2
Fitted parameters corresponding to the hyperfine interactions (Hfi1, Hfi2, and Hfi3) observed at RT in air for m-HfO_2 and Samples I–IV. f_i and δ_i are expressed in % and ω_{Qi} in Mrad/s.

Sample	Preparation treatment	Hfi1				Hfi2				Hfi3			
		f_1	ω_{Q1}	η_1	δ_1	f_2	ω_{Q2}	η_2	δ_2	f_3	ω_{Q3}	η_3	δ_3
m-HfO_2	Irradiated initial powder annealed in air at 1123 K (1 h)	100	125.2(3)	0.350(4)	3.8(2)								
Sample I	Manually mixed powders treated in air at 1273 K (26 h) + 1523 K (6 h)	100	123.7(4)	0.361(5)	4.7(3)								
Sample II	Sample I ball-milled 3 h at 40 Hz	90(2)	125.1(9)	0.371(9)	9.3(5)	6(2)	136(1)	0.57(2)	1(1)	4(1)	197(1)	0.17(4)	1(1)
Sample III	Sample II annealed in air at 1273 K (26 h) + 1523 K (6 h)	9(1)	121(1)	0.01(9)	2(2)	55(5)	118(5)	0.58(6)	17(3)	36(5)	207(2)	0.17(3)	6(1)
Sample IV	Sample II pressed as pellet + the same thermal annealing done in Sample III	25(6)	122(1)	0.0(1)	3(1)	54(2)	113(4)	0.71(3)	12(2)	21(5)	207(2)	0.17(2)	3(1)

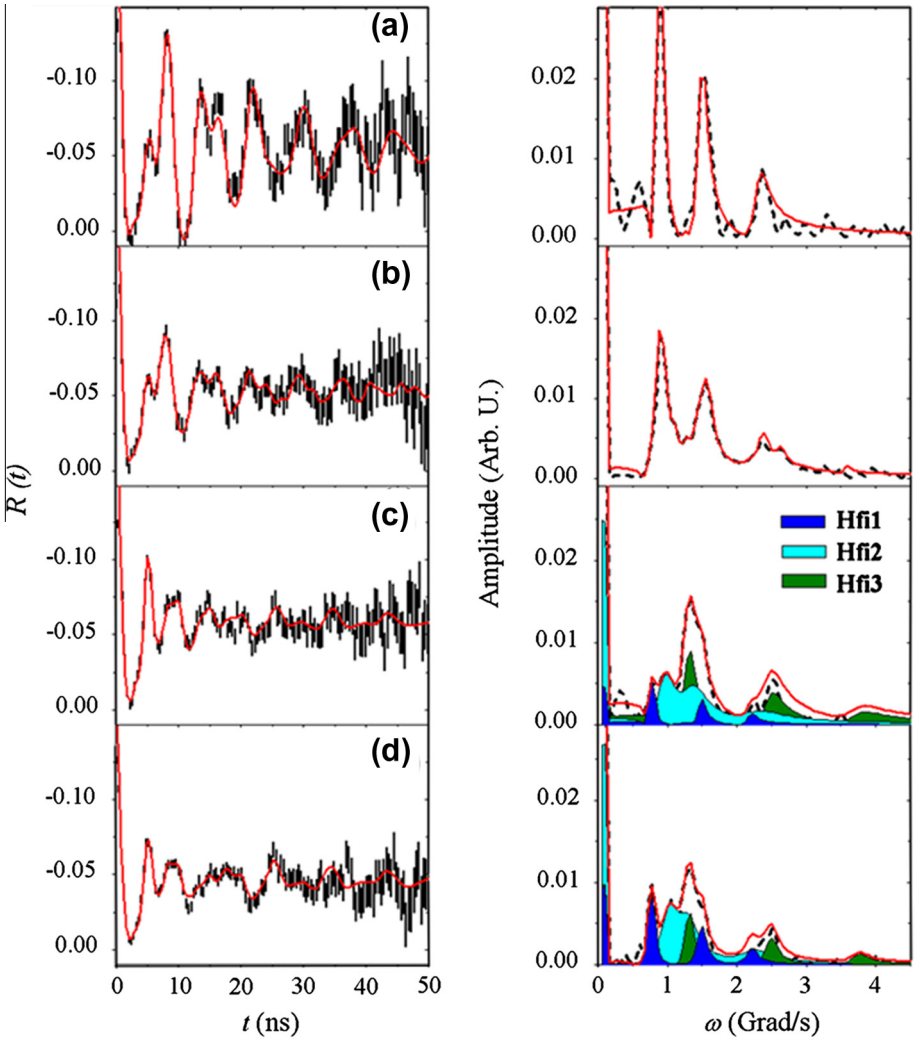

Fig. 4. $R(t)$ spectra (left) and their corresponding Fourier transformed spectra (right) for ^{181}Ta probes in (a–d) Samples I–IV (see Section 2.4), respectively, taken at RT in air. On the right, the ω_n frequencies corresponding to hyperfine interactions Hfi1, Hfi2, and Hfi3 are depicted.

departure was already observed in PAC experiments performed on other *bixbyites* in which the ^{181}Hf($\rightarrow^{181}$Ta) tracers were introduced in the samples by ion implantation [47–52]. Finally, both interactions HfiC and HfiD account to 100% of the $R(t)$ spectra along the whole temperature range of measurement, with the exception that two minor interactions amount to less than 25% of the probes. The spurious interactions HfiX and HfiY, whose hyperfine parameters are now reported in Table 1, were observed in the temperature range RT-473 K [47]. Due to the temperature range in which these two interactions are observed and the hygroscopic tendency of rare-earth sesquioxides, the possibility of desorption–absorption of water in the samples was investigated. However, a Differential-Thermal Analysis (DTA) carried out for the Ho_2O_3 samples did not confirm this hypothesis.

Under all these evidences, HfiC and HfiD can be assigned to ^{181}Ta atoms localized at the defect-free cationic sites *C* and *D* of the Ho_2O_3 *bixbyite* crystalline structure.

First, let us briefly discuss the results obtained with the irradiated *m*-HfO_2 initial powder. The fitted hyperfine parameters for this powder agree with those reported in the literature for the dominant quadrupole interaction assigned to ^{181}Ta impurities localized at defect-free cation sites in polycrystalline HfO_2 [45,46] (see Table 2). First-principles electronic structure calculations have shown that this interaction corresponds to ^{181}Ta donor impurities localized at these cationic sites [8].

The $R(t)$ spectra and their corresponding Fourier transforms, taken on Samples I–IV are presented in Fig. 4. Three hyperfine interactions were necessary to describe these $R(t)$ spectra: Hfi1, Hfi2, and Hfi3, their parameters being displayed for each sample in Table 2. In the case of Sample I (Fig. 4a), only Hfi1 was observed. From the three possible sources for a single observed interaction

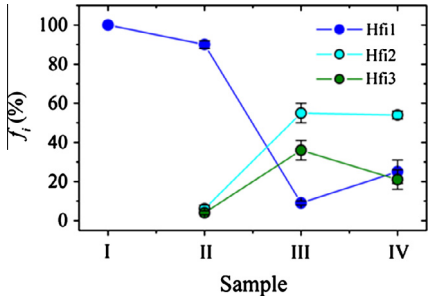

Fig. 5. Evolution of the fractions of hyperfine interactions Hfi1, Hfi2, and Hfi3 (see Table 2) for Samples I–IV (see Section 2.4).

(Hf totally doping Ho_2O_3, Ho saturating the HfO_2 host, or unperturbed HfO_2), their hyperfine parameters correspond to those of ^{181}Ta in pure *m*-HfO_2. In Sample I (manually mixed powder), the thermal treatment at rather high temperatures was not enough to start the Hf diffusion into the Ho_2O_3 lattice.

After 3 h of ball milling, important changes occur. In effect, the Fourier spectrum of Sample II (Fig. 4b) shows basically the peaks associated with pure *m*-HfO_2 but, in addition, a broadening of these peaks can be observed and two additional interactions were necessary to reproduce the experimental $R(t)$ spectrum. The first interaction, which accounts for about 90% of the pattern, is very similar to that obtained for pure *m*-HfO_2, but the increment of its distribution (see Table 2) indicates the presence of some degree of disorder in the environment of the probes still located at cationic sites of *m*-HfO_2. In the case of the other two interactions, the more populated one (Hfi2) is characterized by a large η value. On the other hand, Hfi3 presents η close to zero, and the frequency associated with this interaction is twice as large as the asymmetric one (see Table 2). From their comparison with HfiC and HfiD of the implanted samples, we tentatively associate these two interactions with probes located at the crystalline nonequivalent cation sites *C* and *D* of Ho_2O_3, respectively, but with a high degree of local disorder. Considering the relative fractions of the hyperfine interactions, up to 10% of Ho ions could be doping the HfO_2 host. This may produce the mentioned disorder (δ_1 = 10%) that can be originated from different scenarios such as substitutional Ho ions randomly localized at Hf sites, at interstitial sites or by oxygen vacancies that are favored by the presence of an acceptor impurity such as Ho in HfO_2.

In the case of Sample III (Fig. 4c), the spectrum changes drastically. In effect, the interaction previously associated with *m*-HfO_2 (Hfi1) reduces its population from 90% to 9%. In addition, it is clear that the cation neighborhood in *m*-HfO_2 is distorted, as shown by the noticeable change in the hyperfine parameters of Hfi1. In particular, the η value departs from that of crystalline *m*-HfO_2 (see Table 2). The hyperfine parameters that characterize Hfi2 and Hfi3, which increased their population up to 91%, are very similar to those found in the PAC experiments performed on the implanted samples (see HfiC and HfiD in Table 1). Nevertheless, the η value of Hfi3 differs from that expected according to the axial symmetry of site *D* and the EFG distributions of Hfi2 and Hfi3 are still rather high. These facts show that the ball milling plus the thermal treatment are necessary to obtain a high degree (91%) of Hf substitution in the Ho_2O_3 lattice by Hf diffusion, once the *m*-HfO_2 structure is destabilized (occurred in Sample II). It is interesting to note that the increment in the amount of exchanged Hf ions does not change the relative Hf population of sites *C* and *D*, f_{Hfi2}/f_{Hfi3} = 1.5, smaller than the value of 2.3 obtained in the ^{181}Hf-implanted samples after annealing (see Table 1). This preference of the Hf impurities for site *D* was already observed in different stages of the ionic exchange of Hf ions in Tm_2O_3 [36].

In Sample IV, the pressure effect followed by the same annealing treatment carried out in Sample III originates interesting changes in the spectrum (Fig. 4d). First, the amount of Hf ions exchanged into the Ho_2O_3 host is lower than that observed in Sample III (see Table 2 and Fig. 5). However, the hyperfine parameters of Hfi1 remain almost the same. On the other hand, the ratio f_{Hfi2}/f_{Hfi3} increases up to 2.6, being this value very close to that expected (f_C/f_D = 3) for an homogenous Hf distribution at the cationic sites and also in agreement with the value obtained in the implanted samples. However, the preference for the population of site *D* (i.e., f_C/f_D < 3) is maintained. The pressure effect also produces a 30% decrease of the EFG distribution of Hfi2 and 50% in Hfi3, pointing to a free-of-defect environment for the ^{181}Ta impurities. Finally, ω_Q and η that characterize Hfi2 and Hfi3 agree very well with the results obtained in the ^{181}Hf-implanted Ho_2O_3 sample (HfiC and HfiD in Table 1). In addition, these values also agree very well with the prediction of the previously established ^{181}Ta EFG systematics for rare-earth *bixbyites* (see Fig. 4 in Ref. [36]).

The measurements at 573 K carried out on Samples III and IV showed, as expected, the same hyperfine interactions observed at RT. The hyperfine parameters of Hfi2 and Hfi3 present the same temperature dependence that HfiC and HfiD showed in the implanted samples. It is interesting to note here that in the temperature range RT-573 K, in which the spurious interactions HfiX and HfiY were present in ^{181}Hf-implanted Ho_2O_3 (see Table 1), no additional interactions are present in these samples doped by ball-milling. At this point, we can undoubtedly assign Hfi2 and Hfi3 to ^{181}Ta probes localized at defect-free cations sites *C* and *D*, respectively, of the Ho_2O_3 structure.

From the theoretical point of view, up to our knowledge there are not EFG predictions at Ta impurity sites in lanthanide sesquioxides that could confirm these assignments. In this sense, we performed *ab initio* electronic structure calculations in Ho_2O_3:Ta using the Augmented Plane Waves plus local orbital (APW + lo) method [53] embedded into the WIEN2k code [54]. The ^{181}Ta dilution was simulated substituting one Ho atom at sites *C* or *D* from the unit cell by a Ta atom, giving a cationic dilution of 6.25%. For this concentration, Ta behaves as an isolated impurity. Exchange and correlation effects were treated using the local density approximation (LDA). We checked the results using the LDA + U approximation in order to describe correctly the insulator character of these oxides [55], giving basically the same results. The parameter RK_{max}, which controls the size of the basis set, was set to 6. Integration in the reciprocal space was performed using the tetrahedron method considering 100 *k* points in the first Brillouin zone. A detailed description of the calculation procedure can be found in Ref. [55]. We studied two charge state of the impurity taking into account the Ta double donor character in this oxide: the *neutral state* obtained replacing a Ho atom by a Ta atom and the *charged state* removing two electrons from the cell. In both cases, we took into account the structural relaxations of all atoms of the cell. Since for this impurity–host system the results are independent of the impurity charge state, we report the results of the *charged state*. Ta introduces contractions in the Ta–O_{NN} bond-lengths, 8% and 10% at sites *C* and *D*, respectively. In the case of site *C*, the relaxations are slightly anisotropic. The predicted ω_Q and η values at site *C* (*D*) are 125 (207) Mrad/s and 0.6 (0.0), respectively, in excellent agreement with the experimental results (see Tables 1 and 2).

All these agreements show the capability of this mechanochemical solid-state reaction process between Ho_2O_3 and *m*-HfO_2 to locate more than 75% of the Hf ions at defect-free cation sites of the sesquioxide.

In addition, the *ab initio* calculations can also explain the relative Hf preference to populate the cationic site *D* in Ho_2O_3 and Tm_2O_3, which was observed with different degrees in all the ^{181}Hf-doped Ho_2O_3 and Tm_2O_3 [36] PAC experiments. We performed *ab initio* total energy calculations for Hf-doped Ho_2O_3 and Tm_2O_3 in which a Hf atom occupies alternatively the two possible cation sites. We are assuming that ^{181}Hf atoms do not change sites after their radioactive decay to ^{181}Ta. The calculations were performed with the same Hf dilution as that used in the case of the Ta-doped Ho_2O_3 and with the same precision. After relaxation of the doped structures we obtained the same energy (within the convergence error) for Hf localized at sites *C* and *D* in Ho_2O_3, while in Tm_2O_3 an energy difference of 0.014 eV shows that Hf at site *D* is the more stable situation. These results are in agreement with the nearly homogeneous experimental Hf distribution among both cationic sites (f_C/f_D = 2.6) obtained in the case of Ho_2O_3 and with the much lower value (f_C/f_D = 1.9) observed for Tm_2O_3 [36].

Let us finally discuss the possible scenarios corresponding to Hfi1 in Samples II–IV. In Sample II, after 3 h of high-energy ball

milling, ω_Q and η of Hfi1 remain almost unchanged. PAC experiments on activated m-HfO_2 powder [56] after 3 h of milling showed that the η parameter of the hyperfine interaction corresponding to the monoclinic phase increases from 0.36 to 0.5, in addition to the development of a new interaction, characterized by ω_Q = 190 Mrad/s, η = 0.5–0.7, and δ = 18%. This interaction was assigned to a tetragonalization of the monoclinic phase [56]. None of these two interactions corresponds to Hfi1 in Sample II. The large amount of Ho_2O_3 powder with respect to that of HfO_2 in our samples, which can supply a kind of wrapping protection upon hitting, could explain the constancy of Hfi1 after 3 h of milling. On the other hand, the tetragonalization observed in Ref. [56] could have been produced by Fe impurities coming from the Fe vial and balls used. In our samples, the agate vial and ball prevent from this contamination.

On the other hand, the increment of the EFG distribution of Hfi1 can be due to: (a) the production of oxygen vacancies distributed distantly from the Hf atoms; (b) the distribution of Ho atoms at the cationic next-nearest-neighbors (NNN) shell, since up to only 10 at.% concentration of Ho atoms can be present after the Ho-doping of the HfO_2 matrix at this stage; and (c) a combination of (a and b). With this low concentration of defects, there is a high probability that they would be localized beyond the second atomic coordination shell of the Ta probe and, as it is well known, their contribution to the EFG will be very small due to the r^{-3} EFG's dependence.

Besides this, the rather low EFG distribution enables an estimation of the minimum grain size of the sample subjected to ball-milling. An EFG distribution of 10% cannot hide a second interaction originated from Ta atoms localized at the grain surface, since EFGs at surface sites can be 5–10 times larger than the bulk EFG [57,58]. This kind of interaction, if present, should have an intensity lower than 1%, the lower fraction that a PAC experiment can resolve. Thus, considering a ratio of 1% between Hf atoms localized at the surface and at the bulk, a rough estimation gives a lower limit of 30 nm for the mean grain diameter.

The great modification of Hfi1 parameters occurred when a strong ionic exchange between Hf and Ho was produced (Samples III and IV) or, at least, when 75–90% of Hf atoms doped the Ho_2O_3 matrix. The destabilization of the Ho_2O_3 and HfO_2 lattices or the close contact of the nanostructured powders produced by the ball-milling process enable to develop an efficient ionic exchange by means of a subsequent thermal treatment. This process decreases greatly the η parameter and the EFG distribution of Hfi1 (see Table 2). If the Ho atoms would have been segregated, ^{181}Hf ions were not diffused into metallic Ho, since the characteristic hyperfine interaction of ^{181}Ta in metallic Ho (ω_Q = 50–60 Mrad/s, η = 0 [59,60]) is not present in Samples III and IV. On the other side, the change in the η parameter together with a very low EFG distribution is compatible with a high doping concentration of Ho atoms into the HfO_2 host. In effect, considering a homogenous Ho distribution, the NNN shell from Ta should be saturated by Ho atoms, hence all Ta atoms would sense the same EFG. The Ho atoms, which has a larger ionic radius than Hf [61], should produce structural relaxations on its O_{NN}'s bond-lengths, thus increasing (through the oxygen atoms shared by Ho and Ta) the contractions produced naturally by the Ta atoms in the HfO_2 host, which are predicted by *ab initio* electronic structure calculations [8]. These additional bond-length contractions between Ta and its O_{NN} could be at the origin of the η parameter change. The slight variation of ω_Q in Samples III and IV is in agreement, within this scenario, with the additional Ta–O_{NN} bond-length small contractions and with the fact that the NN Ho atoms have strongly localized electrons that are far enough from the Ta atoms, and therefore do not contribute to the EFG [55]. A low concentration of Ho atoms into HfO_2 trapped near the Ta site should be discarded since this should have produced a higher EFG distribution.

Finally, we want to comment on previous results obtained applying the same Hf doping method into the isostructural semiconductor Tm_2O_3 [36]. Tm_2O_3 has a lattice parameter a slightly smaller (1.5%) than that of Ho_2O_3. Milling times of 6 h were necessary to achieve a 60% Hf substitution at free-of-defect cationic sites of Tm_2O_3. This result shows that the lattice parameter (in other words, the available space at the cationic sites) also plays an important role in the doping process. It is worth mentioning that even though, in the case of Tm_2O_3:^{181}Ta, the hyperfine parameters agree with the ^{181}Ta EFG systematics [36], the Ho_2O_3:^{181}Ta case is the first one in which the ball milling results can be compare with those coming from ^{181}Ta-implanted experiments and with *ab initio* EFG calculations, giving an strong support to the efficiency of the ball-milling doping method.

If we compare the hyperfine parameters of Hfi1 (see Table 2) with those previously obtained for the HfO_2–Tm_2O_3 system [36], we see that Hfi1 has the same hyperfine parameters at the final stage of the doping process in both blends, but with a different exchange rate in samples with similar history. In the case of Tm_2O_3, an additional ball milling cycle was needed before the thermal treatment could produce the drastic changes in Hfi1 parameters. The similarity of Ho and Tm ionic radii is in agreement with the proposed scenario in which these impurities are located at the NNN shell from ^{181}Ta and producing similar contractions at the ^{181}Ta–O_{NN} bond-lengths, thus originating the same EFG in both cases. This result is also in agreement with the highly localized electron density of Ho and Tm atoms situated far enough from the ^{181}Ta atom.

4. Conclusions

The doping method described in this paper enabled that 75–90 at.% of Hf atoms dope the Ho_2O_3 lattice, achieving 0.90–1.08 at.% cationic doping concentration. The PAC measurements showed that the Hf impurities are localized at substitutional defect-free cation sites of this structure. An almost homogeneous distribution of the Hf ions into the Ho_2O_3 host was obtained under pressure. In addition, the spurious hyperfine interactions found in ^{181}Hf-implanted Ho_2O_3 samples were not produced by this doping method, giving a cleaner characterization of the EFG. The successful study of this phase through this particular doping method enables broader studies of potential phases that can arise at the interphase of HfO_2/Ho_2O_3 stack systems.

At the final stage of the solid-state reaction, the parameters of the dominant hyperfine interactions, assigned to ^{181}Ta probes located at both cation sites of Ho_2O_3, are in excellent agreement with those determined with ^{181}Hf-implanted Ho_2O_3 samples, to those predicted by the ^{181}Ta EFG systematics established in rare-earth *bixbyites* doped by ion-implantation of ^{181}Hf($\rightarrow^{181}$Ta) ions, and with *ab initio* EFG predictions. This agreement, together with the Tm_2O_3:^{181}Ta experimental results [36], show the capability of this solid-state reaction method to locate the impurities at free-of-defects cation sites of the sesquioxide and, probably, for all lanthanides with a > 10.45 Å. In addition, the highly localized information obtained in the PAC experiments and their nature enable us to follow and quantify, in a model-independent way, the absolute efficiency of the doping process and to determine the role played by each step of the method and how the milling times, the thermal treatments and the pressure can influence the ionic exchange.

Along the ionic exchange process, a third hyperfine interaction was clearly characterized. Before the strong Hf diffusion into Ho_2O_3, this interaction was assigned to ^{181}Ta probes localized at Hf sites in m-HfO_2, with a distribution of defects (oxygen vacancies

or Ho impurities) localized beyond the cationic NN shell. After the strong Hf doping in Ho_2O_3, this interaction presented an apparent modification of its parameters, being ascribed to ^{181}Ta atoms at *m*-HfO_2 cation sites having their NNN shell saturated by Ho atoms. The slight decrease of the EFG and the change in the asymmetry parameter is well correlated with the additional contractions in the Ta–O_{NN} bonds originated in the outward relaxations that the Ho impurities should produce in the Ho–O_{NN} bonds, when Ho are substituting Hf atoms belonging to the NNN shell of the ^{181}Ta site.

Our results show that high-energy milling together with high temperature treatments are both necessary to achieve a high degree of Hf substitution in the cation sublattice of the Ho_2O_3 structure. In the same way, comparison with the results obtained for Tm_2O_3 shows that the necessary milling time to achieve this goal depends on the available size at the cationic sites. We conclude that for larger lattice parameters, smaller milling times, together with subsequent thermal treatments, should be sufficient to obtain a high degree of Hf substitution in the oxide lattices. In addition, we showed that the pressure effect onto the crystal structure favors the impurity substitution at cationic sites closer to a homogenous distribution of the probes and with much less local and far disorder. *Ab initio* total energy calculations also showed the Hf preference to populate the symmetric site *D* in the case of Tm_2O_3 and the nearly homogeneous Hf distribution among both cationic sites obtained in the case of Ho_2O_3, in good agreement with the PAC experiments.

Finally, the hyperfine interaction that characterizes the *m*-HfO_2 phase heavily doped with Ho acceptor impurities is almost coincident with that already observed at the final stage of the solid-state reaction between *m*-HfO_2 and Tm_2O_3, fact well correlated with the high localization of the lanthanide electron density and the similar structural relaxations that Ho and Tm impurities may be introducing into the *m*-HfO_2 lattice. This interaction may be expected to be observed in future PAC studies of HfO_2/Ho_2O_3 interphases produced by this or other methods, with different relative concentrations of the starting oxides.

Acknowledgments

This work was partially supported by Consejo Nacional de Investigaciones Científicas y Técnicas (CONICET) under Grant No. PIP0002, Argentina, and the Third World Academy of Sciences (TWAS), Italy (RGA 97-057). The ^{181}Hf implantations carried out at the H-ISKP of Bonn University (Germany) are kindly acknowledged. This research made use of the HP-Parallel-Computing Bose Cluster, and the computational facilities of the Physics of Impurities in Condensed Matter (PhI) group at IFLP and Departamento de Física (UNLP), and the HUGE cluster, Aarhus University, Aarhus, Denmark. G.N.D., L.A.E, and M.R. are members of CONICET, Argentina.

References

[1] Y. Muto, S. Nakatomi, N. Oka, Y. Iwabuchi, H. Kotsubo, Y. Shigesato, Thin Solid Films 520 (2012) 3746–3750.
[2] S. Wang, Y. An, D. Feng, Z. Wu, J. Liu, J. Appl. Phys. 113 (2013) 153901.
[3] A. Sasahara, M. Tomitori, J. Phys. Chem. C 117 (2013) 17680–17686.
[4] L.A. Errico, G. Fabricius, M. Rentería, P. de la Presa, M. Forker, Phys. Rev. Lett. 89 (2002) 055503.
[5] L.A. Errico, G. Fabricius, M. Rentería, Phys. Rev. B 67 (2003) 144104. and refs. therein.
[6] G.N. Darriba, L.A. Errico, P.D. Eversheim, G. Fabricius, M. Rentería, Phys. Rev. B 79 (2009) 115213.
[7] S. Decoster, S. Cottenier, B. De Vries, H. Emmerich, U. Wahl, J.G. Correia, A. Vantomme, Phys. Rev. Lett. 102 (2009) 065502.
[8] M.A. Taylor, R.E. Alonso, L.A. Errico, A. López-García, P. de la Presa, A. Svane, N.E. Christensen, Phys. Rev. B 82 (2010) 165203.
[9] G.N. Darriba, M. Rentería, H.M. Petrilli, L.V.C. Assali, Phys. Rev. B 86 (2012) 075203.
[10] T. Wiktorczyk, Thin Solid Films 405 (2002) 238–242.
[11] C.T. Au, K.D. Chen, H.X. Dai, Y.W. Liu, J.Z. Luo, C.F. Ng, J. Catal. 179 (1998) 300–308.
[12] Z. Ma, S.H. Overbury, S. Dai, J. Mol. Catal. A: Chem. 273 (2007) 186–197.
[13] A.A. Frolov, Y. Frolov, E.R. Andrievskaya, J. Eur. Ceram. Soc. 30 (2010) 2497–2504.
[14] Y. Ledemi, D. Manzani, S.J.L. Ribeiro, Y. Messaddeq, Opt. Mater. 33 (2011) 1916–1920.
[15] T. Wiktorczyk, J. Electrostat. 51 (2001) 131–136.
[16] M. Leskela, K. Kukli, M. Ritala, J. Alloys Comp. 418 (2006) 27–34.
[17] M. Fanciulli, G. Scarel, Rare Earth Oxide Thin Film: Growth Characterization and Applications, Springer, Berlin, 2007.
[18] Y. Xiong, H. Tu, J. Du, X. Zhang, D. Chen, W. Wang, Appl. Phys. Lett. 98 (2011) 082906.
[19] X. Wang, X. Zhang, Y. Xiong, J. Du, M. Yang, L. Wang, H. Tu, Mater. Sci. Forum 687 (2011) 209–214.
[20] T.M. Pan, M. Huang, Mater. Chem. Phys. 129 (2011) 919–924.
[21] T.M. Pan, W. Chang, F. Chiu, Thin Solid Films 519 (2010) 923–927.
[22] H. Frauenfelder, R.M. Steffen, in: K. Siegbahn (Ed.), Alpha-, Beta-, and Gamma-Ray Spectroscopy, vol. 2, North-Holland, Amsterdam, 1966, pp. 997–1195.
[23] E.N. Kaufmann, R.J. Vianden, Rev. Mod. Phys. 51 (1979) 161–214.
[24] G. Schatz, A. Weidinger, Nuclear Condensed Matter Physics: Nuclear Methods and Applications, Wiley, Chichester, 1996.
[25] T. Klas, J. Voigt, W. Keppner, R. Wesche, G. Schatz, Phys. Rev. Lett. 57 (1986) 1068–1071.
[26] A. Lerf, T. Butz, Angew. Chem. Int. Ed. Engl. 26 (1987) 110–126.
[27] R. Vianden, U. Feuser, Phys. Rev. Lett. 61 (1988) 1981–1984.
[28] N. Achtziger, W. Witthuhn, Phys. Rev. B 47 (1993) 6990–7004.
[29] J. Meersschaut, C. L'abbé, M. Rots, S.D. Bader, Phys. Rev. Lett. 87 (2001) 107201.
[30] J.M. Ramallo-López, M. Rentería, E.E. Miró, F.G. Requejo, A. Traverse, Phys. Rev. Lett. 91 (2003) 108304.
[31] M. Forker, S. Muller, P. de la Presa, A.F. Pasquevich, Phys. Rev. B 68 (2003) 014409.
[32] F.C.D.A. Lima, R.R. Nascimento, M.B. Gonçalves, S. Cottenier, M.J. Caldas, H.M. Petrilli, Hyperfine Interact. 197 (2010) 23–27.
[33] C.Y. Chain, M. Ceolin, A.F. Pasquevich, Hyperfine Interact. 181 (2008) 99–106.
[34] C.Y. Chain, A.F. Pasquevich, Hyperfine Interact. 197 (2010) 341–346.
[35] A.F. Cabrera, F.H. Sánchez, Phys. Rev. B 65 (2002) 094202.
[36] E.L. Muñoz, G.N. Darriba, A.G. Bibiloni, L.A. Errico, M. Rentería, J. Alloys Comp. 495 (2010) 532–536.
[37] C.Y. Chain, L.C. Damonte, S. Ferrari, E. Muñoz, C. Rodríguez Torres, A.F. Pasquevich, J. Alloys Comp. 495 (2010) 527–531.
[38] C.Y. Chain, R.A. Quille, A.F. Pasquevich, J. Alloys Comp. 495 (2010) 524–526.
[39] M. Rentería, A.G. Bibiloni, G.N. Darriba, L.A. Errico, E.L. Muñoz, D. Richard, J. Runco, Hyperfine Interact. 181 (2008) 145–155.
[40] L.A. Mendoza-Zélis, A.G. Bibiloni, M.C. Caracoche, A.R. López-García, J.A. Martínez, R.C. Mercader, A.F. Pasquevich, Hyperfine Interact. 3 (1977) 315–320.
[41] N. Maslen, V.A. Streltsov, N.A. Ishizawa, Acta Cryst. B 52 (1996) 414–422.
[42] L. Eyring, in: K.A. Gschneider, L. Eyring (Eds.), Handbook on the Physics and Chemistry of Rare Earths, vol. 3, North-Holland, Amsterdam, 1979, pp. 337–400.
[43] Yu.K. Voronko, A.A. Sobol, V.E. Shukshin, Phys. Solid State 49 (2007) 1963–1968.
[44] R.E. Hann, P.R. Suitch, J.L. Pentecost, J. Am. Ceram. Soc. 68 (1985). C-285–286.
[45] A. Ayala, R. Alonso, A. López-García, Phys. Rev. B 50 (1994) 3547–3552.
[46] M. Forker, P. de la Presa, W. Hoffbauer, S. Schlabach, M. Bruns, D.V. Szabó, Phys. Rev. B 77 (2008) 054108.
[47] L.A. Errico, M. Rentería, A.G. Bibiloni, K. Freitag, Physica B 389 (2007) 124–129.
[48] A.F. Pasquevich, A.G. Bibiloni, C.P. Massolo, M. Rentería, J.A. Vercesi, K. Freitag, Phys. Rev. B 49 (1994) 14331–14336.
[49] M. Rentería, F.G. Requejo, A.G. Bibiloni, A.F. Pasquevich, J. Shitu, K. Freitag, Phys. Rev. B 55 (1997) 14200–14207.
[50] M. Rentería, A.G. Bibiloni, F.G. Requejo, A.F. Pasquevich, J. Shitu, L.A. Errico, K. Freitag, Mod. Phys. Lett. B 12 (1998) 819–827.
[51] L.A. Errico, M. Rentería, A.F. Pasquevich, A.G. Bibiloni, K. Freitag, Eur. Phys. J. B 22 (2001) 149–156.
[52] M. Rentería, K. Freitag, L.A. Errico, Hyperfine Interact. 120–121 (1999) 449–455.
[53] E. Sjöstedt, L. Nordström, D.J. Singh, Solid State Commun. 114 (2000) 15; G.K.H. Madsen, P. Blaha, K. Schwarz, E. Sjöstedt, L. Nordström, Phys. Rev. B 64 (2001) 195134.
[54] P. Blaha, K. Schwarz, G. Madsen, D. Kvasnicka, J. Luitz, WIEN2k, An Augmented Plane Wave Plus Local Orbitals Programfor Calculating Crystal Properties, Karlheinz Schwarz, Technical Universität Wien, Austria, 1999.
[55] D. Richard, E.L. Muñoz, M. Rentería, L.A. Errico, A. Svane, N.E. Christensen, Phys. Rev. B 88 (2013) 165206.
[56] C.Y. Chain, S. Ferrari, L.C. Damonte, J.A. Martínez, A.F. Pasquevich, J. Alloys Comp. 536s (2012) s50–s54.
[57] G.N. Darriba, R. Faccio, M. Rentería, Physica B 407 (2012) 3093–3095.
[58] G.N. Darriba, R. Faccio, M. Rentería, unpublished results.
[59] M. Forker, W. Steinborn, Phys. Rev. B 20 (1979) 1–9.
[60] R.L. Rasera, B.D. Dunlap, G.K. Shenoy, Phys. Rev. Lett. 41 (1978) 1188–1191.
[61] R.D. Shannon, Acta Cryst. A32 (1976) 751–767.